Inorganic Chemistry

ARTICLE

pubs.acs.org/IC

Structure and Magnetism of the Quasi-1-d $K_4Cu(MoO_4)_3$ and the Structure of $K_4Zn(MoO_4)_3$

Melissa C. Menard,[†] Rieko Ishii,[‡] Satoru Nakatsuji,[‡] and Julia Y. Chan*[,†]

[†]Department of Chemistry, Louisiana State University, Baton Rouge, Louisiana 70803, United States

[‡]Institute for Solid State Physics, University of Tokyo, Kashiwa 277-8581, Japan

Supporting Information

ABSTRACT: Single crystals of $K_4Cu(MoO_4)_3$ and nonmagnetic $K_4Zn(MoO_4)_3$ have been grown by the flux-growth method. $K_4Cu(MoO_4)_3$ can be described as a quantum quasi-1-d antiferromagnet with correlations between neighboring Cu^{2+} ions but no magnetic long-range ordering down to 0.4 K. Comparison of the structure and magnetic properties of isostructural $A_4Cu(MoO_4)_3$ (A = K, Rb) allows the isolation of the effects of low dimensionality from structural distortion along the Cu−O−Mo chains. The characteristic one-dimensional behavior is hence suppressed to lower the temperature in $K_4Cu(MoO_4)_3$ in comparison with that of the Rb analogue. For example, a broad peak in the specific heat is observed ∼2.3 K at 0 T, which is consistent with the onset of the quantum spin liquid state.

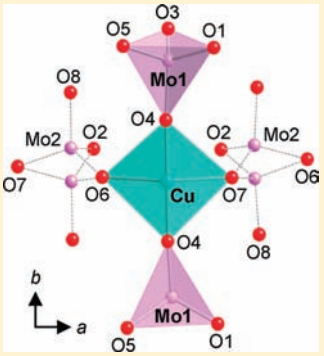

INTRODUCTION

The low dimensionality and quantum fluctuations found in quantum magnets with S = 1/2 and S = 1 present a unique opportunity to discover new states of matter. Examples of these new states of matter include Haldane gap formation (spin gap),[1−3] quantum spin liquid,[4,5] 2D frustrated antiferromagnets,[6] and Bose−Einstein condensate (superfluid).[7] Quantum magnets can be generally classified as materials with strong magnetic correlations that fail to show long-range order down to T = 0 K due to quantum fluctuations. The search for model systems to compare experimental results with theoretical predictions has been an exciting quest, and we have focused on the crystal growth and characterization of quantum magnets. This is motivated by the spin-1/2 quantum magnets which present the simplest models for the study of low dimensional materials with enhanced quantum fluctuations. Specifically, many Cu^{2+} (S = 1/2) systems have been found to display quantum behavior such as the quasi-2-d quantum antiferromagnet La_2CuO_4,[4] the quantum spin system $SrCu_2(BO_3)_2$,[8] the metal−organic dimer system, $C_{36}H_{48}Cu_2F_6N_8O_{12}S_2$ exhibiting Bose−Einstein condensation of magnons,[9] the spin ladders, $Sr_{m-1}Cu_{m+1}O_{2m}$, which exhibit a 1-d chain spin liquid ground state,[10] and the spin-1/2 kagome antiferromagnet $Cu_3Zn(OH)_6Cl_2$.[11]

Many Mo-oxides adopt low dimensional structures.[12−24] In these phases, there are distortions in the MoO_4 tetrahedra, which can be explained by electronic considerations. M−Mo-oxide (M^{m+} = transition metal or group 13−14 metal with m < 6) compounds containing MoO_4 tetrahedra typically exhibit corner sharing between the MoO_4 tetrahedra and the M−O metal-centered environments.[15,18−27] In these compounds, Mo−O−M interactions are more favorable than Mo−O−Mo interactions due to the very electron-deficient nature of Mo^{6+} (d^0). Therefore, increased interactions along one direction (Mo−O−M) are enhanced at the expense of the interactions between Mo−O−Mo, along the orthogonal direction. There is also the possibility of second-order Jahn−Teller distortions in the Mo^{6+} environment, which would account for the decreased dimensionality. $RbFe(MoO_4)_2$ and $Rb_4Mn(MoO_4)_3$ are two reported structurally related examples of 2-d triangular antiferromagnets with spin-$^5/_2$ due to the high-spin Fe^{3+} and Mn^{2+}, respectively.[28,29] We have selected to study low dimensional compounds with Mo^{6+} and Cu^{2+}, which may lead to low dimensional materials with quantum fluctuations. Spin-1/2 Cu^{2+} allows for the study of interacting, individual spins without spin−orbital coupling, and Mo^{6+} can provide either a nonmagnetic block to isolate each magnetic moment or an anisotropic pathway for the coupling of magnetic ions through superexchange along a preferred direction.

Dimensionality can be viewed as another adjustable parameter when searching for new materials presenting unique challenges when characterizing new materials. One way to tune dimensionality is by chemical doping to affect coupling between layers/chains. Demonstrating this control often involves tuning at the edge of structural stability and careful adjustment of the synthetic parameters in order to grow phases with inherent structural disorder. Dimensionality, like disorder, is more than just a physical attribute of a material due to the chemical effects on

Received: March 8, 2011
Published: August 18, 2011

local environments. Understanding the effects of dimensionality can lead to better understanding of complex behavior.

The structure of the K-analogue, $K_4Cu(MoO_4)_3$, has been previously reported from X-ray powder data with two reversible structural transitions.[30] The high temperature (~900 K) phase was reported as a metastable phase with a hexagonal unit cell, and the most stable of the three polymorphs, the midrange temperature phase (~700 K), was reported with an orthorhombic unit cell.[30] The low temperature phase (~600 K), although reported as a monoclinic cell, is marked by peak splitting possibly due to twinning and a drastic decrease in crystal quality.[30] All previous reports of the $A_4Cu(MoO_4)_3$ (A = K, Rb, Cs) family indicate that the low temperature phase is likely a supercell of the stable, high temperature hexagonal polymorph, and the orthorhombic phase is a structural variant of the hexagonal polymorph, termed pseudohexagonal.[30] Full structural and property characterization of these phases was not accomplished due to past difficulties in growing high-quality single crystals and in handling hygroscopic crystals. Recently, we discovered $Rb_4Cu(MoO_4)_3$, a quasi-1-d quantum antiferromagnet with quantum fluctuations.[15] When comparing quasi-1-d quantum antiferromagnets, $A_4Cu(MoO_4)_3$ (A = K, Rb), the structural differences that affect the strength of magnetic correlations between Cu^{2+} ions can be investigated to isolate the dimensionality and structural disorder parameters. Here, we report the growth and characterization of single crystals of the orthorhombic phase of $K_4Cu(MoO_4)_3$, a new quasi-1-d quantum antiferromagnet, and the structure of a nonmagnetic reference, $K_4Zn(MoO_4)_3$, and also compare the isostructural $A_4Cu(MoO_4)_3$ (A = K, Rb) compounds to examine the structural differences that affect the strength of magnetic correlations between Cu^{2+} ions.

EXPERIMENTAL SECTION

Synthesis. Polycrystalline samples of $K_4M(MoO_4)_3$ (M = Cu, Zn) were synthesized via the ceramic reaction method according to the chemical reaction

$$2K_2CO_3 + MO + 3MoO_3 \rightarrow K_4M(MoO_4)_3 + 2CO_2\uparrow \quad (M = Cu, Zn)$$

Because of the hygroscopic nature of K_2CO_3, the reactants were dehydrated by heating at 300 °C for over 3 h before grinding. The mixture was pressed into a pellet and calcined at 480 °C for 40 h. The procedure was repeated 3 times to obtain a homogeneous phase. Single crystals were grown using $K_2Mo_2O_7$ as the flux and polycrystalline $K_4M(MoO_4)_3$ (M = Cu, Zn) as the charge with a charge−flux molar ratio of 1:1. Melt solutions were kept under oxygen atmosphere in a fused silica tube at 590−600 °C for 40 h, followed by cooling to 500 at 1 °C/h. Bluish-green, transparent, hexagonal $K_4Cu(MoO_4)_3$ crystals and colorless, transparent, thin $K_4Zn(MoO_4)_3$ crystals were obtained. X-ray powder diffraction was performed to ensure phase purity with a Rigaku RINT 2100 diffractometer (Cu Kα λ = 1.54056 Å).

Structure Determination. Crystals of approximately 0.03 × 0.03 × 0.03 mm^3 and 0.05 × 0.11 × 0.12 mm^3 of $K_4M(MoO_4)_3$ (M = Cu, Zn) sizes, respectively, were mounted with epoxy onto a glass fiber, coated with Paratone-N oil to protect the hygroscopic samples from air and moisture and were placed on a Nonius Kappa CCD X-ray diffractometer (Mo Kα λ = 0.71073 Å). Single-crystal X-ray diffraction data of $K_4M(MoO_4)_3$ (M = Cu, Zn) were collected at 390 K. The temperature was regulated with a warm stream of dry air produced by an Oxford cryostream. The unit cell parameters were determined from images taken at a rotation of 15°φ. The structure was solved by SIR92[31] and refined by direct methods against F^2 by full-matrix least-squares techniques using SHELXL97.[32] The data were corrected for absorption, and the model was refined with anisotropic displacement parameters. Crystallographic data, atomic positions, and selected bond distances are provided in Tables 1, 2, and 3, respectively. The lattice dimensions of $K_4Zn(MoO_4)_3$ are similar to previously published orthorhombic $K_4Zn(MoO_4)_3$, which was modeled in the space group $P2_12_12_1$.[19] Modeling in the space group $P2_12_12_1$ resulted in missing symmetry when checked with PLATON.[33] Therefore, we report the orthorhombic phases $K_4M(MoO_4)_3$ (M = Cu, Zn) modeled in the space group *Pnma*.

Table 1. Crystallographic Data Table for $K_4Cu(MoO_4)_3$ and $K_4Zn(MoO_4)_3$ (Orthorhombic, *Pnma*)

crystal data		
composition	$K_4Cu(MoO_4)_3$	$K_4Zn(MoO_4)_3$
a (Å)	10.3520(6)	10.68800(10)
b (Å)	22.8070(7)	22.0220(10)
c (Å)	5.9380(10)	6.1050(10)
V (Å^3)	1402.0(3)	1436.9(3)
Z	4	4
crystal size (mm^3)	0.03 × 0.03 × 0.03	0.05 × 0.11 × 0.12
data collection		
temperature (K)	390	390
measured reflections	4346	3843
independent reflections	2469	2160
reflections with $I > 2\sigma(I)$	1623	1600
R_{int}	0.0371	0.0202
h	−15 → 15	−14 → 15
k	−33 → 34	−30 → 31
l	−8 → 8	−8 → 8
refinement		
θ range (deg)	3.55−32.04	1.85−30.04
$R_1[F^2 > 2\sigma F^2)]^a$	0.0397	0.0391
$wR_2(F^2)^b$	0.0974	0.1177
refined parameters	107	107
GoF on F^2	1.061	1.149
μ (mm^{-1})	5.355	5.414
$\Delta\rho_{max}$ (eÅ^{-3})	0.831	3.312
$\Delta\rho_{min}$ (eÅ^{-3})	−0.851	−1.232
extinction coefficient (×10^{-4})	13(3)	8(2)

$^a R_1 = \Sigma||F_0| - |F_c||/\Sigma|F_0|$. $^b wR_2 = [\Sigma w(F_o^2 - F_c^2)^2/\Sigma w(F_0^2)^2]^{1/2}$; $P = (F_o^2 + 2F_c^2)/3$; $w = 1/[\sigma^2(F_o^2) + 0.0422P^2 + 1.2985P]$, $w = 1/[\sigma^2(F_o^2) + (0.0615P)^2 + 1.5504P]$, for $K_4Cu(MoO_4)_3$ and $K_4Zn(MoO_4)_3$, respectively.

Investigation of the structural transitions in $K_4Cu(MoO_4)_3$ yielded an apparent structural transition around 290 K. The reversible transition is similar to that of the previously reported monoclinic phase (~ 12 × 12 × 23 Å^3).[30] This transition is marked by a drastic decrease in crystal quality ($\chi^2 > 5$ and mosaicity ~2) and peak splitting. This phase is stable down to 90 K. Because of the complexity of the structure and the complications arising from poor crystal quality of the low temperature phase, several attempts to solve the low temperature phase of $K_4Cu(MoO_4)_3$ were unsuccessful. We did not observe the reported hexagonal phase in $K_4Cu(MoO_4)_3$ up to 390 K, which is the high temperature limit for our structural determination via single crystal X-ray diffraction, and the experimentally observed phase transition temperatures in $A_4Cu(MoO_4)_3$ (A^+ = K^+, Rb^+, Cs^+) are significantly different from those previously reported by Klevtsov shown in Figure 1.[30]

Magnetic Properties. The magnetic susceptibility of single crystals were measured down to 1.9 K under magnetic fields, B, up to 7 T and the field-dependent magnetization at 2 K was measured up to 7 T with a MPMS SQUID magnetometer to investigate the magnetic properties of

dx.doi.org/10.1021/ic200476n |*Inorg. Chem.* 2011, 50, 8767–8773

Table 2. Atomic Positions of $K_4Cu(MoO_4)_3$ and $K_4Zn(MoO_4)_3$

atom	Wyckoff	*x*	*y*	*z*	occ.[a]	U_{eq} (Å^2)[b]
K1	8*d*	0.66644(11)	0.47425(5)	0.99930(17)	1.00	0.0422(3)
K2	8*d*	0.33352(13)	0.34137(5)	0.9528(2)	1.00	0.0453(3)
Cu	4*c*	0.50186(7)	1/4	0.52051(12)	1.00	0.02838(19)
Mo1	8*d*	0.00243(3)	0.408274(16)	0.01607(6)	1.00	0.02413(13)
Mo2	8*d*	0.67114(7)	0.27229(3)	0.05702(12)	0.50	0.02833(19)
O1	8*d*	0.0896(4)	0.56163(16)	0.1969(6)	1.00	0.0637(11)
O2	4*c*	0.5296(5)	1/4	0.9273(9)	1.00	0.0577(15)
O3	8*d*	0.0615(4)	0.57078(17)	0.7272(6)	1.00	0.0676(12)
O4	8*d*	0.0013(4)	0.33104(16)	0.9812(7)	1.00	0.0748(18)
O5	8*d*	0.1583(4)	0.43451(18)	0.9929(7)	1.00	0.0640(12)
O6	4*c*	0.8076(5)	1/4	0.9174(9)	1.00	0.0566(14)
O7	4*c*	0.1709(4)	1/4	0.1511(7)	1.00	0.0431(11)
O8	8*d*	0.6774(10)	0.3483(4)	1.0366(14)	0.50	0.067(3)
K1	8*d*	0.33335(13)	0.47447(7)	0.4989(2)	1.00	0.0410(3)
K2	8*d*	0.33314(18)	0.65770(6)	0.5213(2)	1.00	0.0440(4)
Zn	4*c*	0.03189(8)	1/4	0.61270(15)	1.00	0.0312(2)
Mo1	8*d*	0.00088(4)	0.593417(19)	0.49846(7)	1.00	0.02391(17)
Mo2	8*d*	0.17304(8)	0.72768(4)	0.99479(14)	0.50	0.0267(2)
O1	4*c*	0.4764(6)	1/4	0.5753(12)	1.00	0.0528(17)
O2	8*d*	−0.0010(5)	0.6741(2)	0.5228(9)	1.00	0.0544(14)
O3	4*c*	0.7127(5)	1/4	0.8044(11)	1.00	0.0471(15)
O4	8*d*	0.1543(4)	0.5674(3)	0.5021(10)	1.00	0.0676(18)
O5	8*d*	0.4283(6)	0.5699(2)	0.2406(9)	1.00	0.0652(15)
O6	8*d*	0.4226(6)	0.5630(2)	0.7785(9)	1.00	0.0653(15)
O7	4*c*	0.7800(6)	1/4	0.2601(10)	1.00	0.0521(16)
O8	8*d*	0.3350(14)	0.3516(5)	0.4811(18)	0.50	0.062(3)

[a] Occupancy. [b] U_{eq} is defined at one-third of the trace of the orthogonalized U_{ij} tensor.

$K_4Cu(MoO_4)_3$. Specific heat, *C*, was measured by the thermal relaxation method down to 0.4 K with a Quantum Design PPMS.

RESULTS AND DISCUSSION

Crystal Structure of $K_4Cu(MoO_4)_3$. $K_4Cu(MoO_4)_3$, shown in Figure 2, is modeled in the orthorhombic *Pnma* space group with lattice dimensions of a = 10.3520(6) Å, b = 22.8070(7) Å, and c = 5.9380(10) Å. Although the structure determination is reported at 390 K, the transition from the low temperature phase to orthorhombic phases occurs at 280 K. The data collected at 390 K are reported here because the crystal quality increased with increasing temperature, and lower temperature data collections were not of sufficient quality to obtain an acceptable structural solution. To ensure phase stability of the orthorhombic phase at room temperature, powder X-ray diffraction was performed, and the data were indexed to the 390 K single crystal model. The structure of $K_4Cu(MoO_4)_3$, shown in Figure 2a, is isostructural with the recently published $Rb_4Cu(MoO_4)_3$.[15] The structure can be described as distorted square planar CuO_4 polyhedra surrounded by two slightly distorted MoO_4 tetrahedra along the *c* direction and two distorted MoO_4 tetrahedra along the *ab*-plane, with partially occupied Mo2 (0.5) and O8 (0.5), as shown in Figure 2b. The Mo1−O distances of the slightly distorted MoO_4 tetrahedra range from 1.725(3) to 1.774(4) Å, which are slightly shorter than those found in $Rb_4Cu(MoO_4)_3$ (from 1.731(6) to 1.780(6) Å). The Mo2−O distances of the distorted, partially occupied MoO_4 tetrahedra range from 1.715(4) to 1.806(4) Å, which are roughly equivalent to those found in $Rb_4Cu(MoO_4)_3$ (1.674(14) to 1.806(12) Å). However, the Mo2−O7 (1.806(4) Å) bond distance in the distorted tetrahedra is significantly longer than the other three Mo2−O bond distances (~1.72 Å).

Table 3. Bond Distances (Å) of $K_4Cu(MoO_4)_3$ and $K_4Zn(MoO_4)_3$

Cu (distorted square planar)		Zn (tetrahedra)	
Cu−O4 (×2)	1.848(4)	Zn−O4 (×2)	1.893(5)
Cu−O7	2.025(4)	Zn−O7	1.995(7)
Cu−O6	2.045(5)	Zn−O6	1.997(6)
Mo1 (Tetrahedra)			
Mo1−O4	1.774(4)	Mo1−O5	1.732(5)
Mo1−O5	1.727(4)	Mo1−O3	1.733(5)
Mo1−O3	1.729(3)	Mo1−O1	1.738(5)
Mo1−O1	1.725(3)	Mo1−O4	1.784(5)
Mo2 (distorted tetrahedra)			
Mo2−Mo2	1.0168(14)	Mo2−Mo2	0.9831(18)
Mo2−O7	1.806(4)	Mo2−O2	1.707(6)
Mo2−O6	1.715(4)	Mo2−O7	1.742(6)
Mo2−O2	1.732(5)	Mo2−O8	1.750(10)
Mo2−O8	1.738(8)	Mo2−O6	1.799(6)
K1−O			
K1−O5	2.761(4)	K1−O8	2.708(11)
K1−O3	2.799(4)	K1−O3	2.761(5)
K1−O1	2.803(4)	K1−O1	2.801(5)
K1−O8	2.884(8)	K1−O5	2.817(5)
K1−O1	2.900(4)	K1−O5	3.158(7)
K1−O6	2.908(5)	K1−O3	3.158(7)
K1−O5	3.061(5)	K1−O1	3.172(7)
K1−O5	3.149(4)	K1−O1	3.210(6)
K1−O1	3.304(4)	K1−O3	3.217(7)
K2−O			
K2−O1	2.800(4)	K2−O2	2.716(4)
K2−O3	2.802(4)	K2−O1	2.761(6)
K2−O5	2.803(4)	K2−O5	2.776(5)
K2−O2	2.913(4)	K2−O3	2.781(5)
K2−O7	2.926(3)	K2−O6	2.886(5)
K2−O6	3.041(4)	K2−O7	2.937(5)
K2−O4	3.117(4)	K2−O4	3.320(6)
K2−O8	3.329(9)	K2−O8	3.339(13)

The Cu^{2+} square planar environment is illustrated in Figure 2c. The two Cu−O1 bonds (1.848(4) Å) of $K_4Cu(MoO_4)_3$, oriented along the *b*-direction, are shorter than the other two Cu−O bonds (Cu−O2 with 2.025(4) Å and Cu−O3 with 2.045(5) Å) (see Figure 2b). The distortions in the MoO_4 tetrahedra and the CuO_4 square planar polyhedra in $K_4Cu(MoO_4)_3$ can be understood by electronic considerations. Mo^{6+} is more electron deficient (electronegative) than Cu^{2+}; therefore, Mo−O−Cu interactions are more favorable than Mo−O−Mo interactions. This is consistent with the longer Cu−O contacts in the *ac*-plane and also the shorter Cu−O contacts along the *b*-axis.

Figure 3 shows the Cu−Mo−O chains in both $A_4Cu(MoO_4)_3$ (A = K, Rb). The ~2.3% shorter distance between chains in

dx.doi.org/10.1021/ic200476n |*Inorg. Chem.* 2011, 50, 8767–8773

$K_4Cu(MoO_4)_3$, as compared to those in $Rb_4Cu(MoO_4)_3$, is consistent with the decrease in lattice parameter, *c*, between the two analogues on moving from $Rb_4Cu(MoO_4)_3$ (6.078(4) Å) to $K_4Cu(MoO_4)_3$ (5.938(4) Å). The Cu−O distances of the distorted square planar CuO_4 polyhedra in $K_4Cu(MoO_4)_3$ range from 1.848(4) to 2.045(5) Å with O−Cu−O angles of 90.01(12)°, 89.87(13)°, 179.3(3)°, and 160.176(3)°. As discussed with respect to $Rb_4Cu(MoO_4)_3$, similar coupling between Cu^{2+} moments is possible through the superexchange mechanism.[15] The Cu^{2+} square planar environment in $K_4Cu(MoO_4)_3$ is shown in Figure 2c. The distance of Cu−O2 (2.432(5) Å) is slightly longer in $K_4Cu(MoO_4)_3$ compared to 2.400(15) Å found in $Rb_4Cu(MoO_4)_3$. This increase in distance between Cu and O2 and the orthogonal orientation between the $d_{x^2-y^2}$ orbital of Cu^{2+} and the p_z orbital of O^{2-} indicates that the superexchange pathway from Cu through O2 is weaker than that found in $Rb_4Cu(MoO_4)_3$, which should make $K_4Cu(MoO_4)_3$ more one-dimensional than $Rb_4Cu(MoO_4)_3$. The *M*−O−*M* bond angles (*M* = Cu or Mo) are shown in Figure 3 with angles along the Cu−O−Mo chains in the K- and Rb-analogues represented in blue and red, respectively. The O−Cu−O bond angles of the Cu^{2+} square planar environment are ∼2% larger than the equivalent angles of the Rb-analogue, which is also consistent with a weaker orbital overlap between Cu and O2. The Mo−O−Cu bond angles along the chain are smaller (∼5%) in $K_4Cu(MoO_4)_3$ compared to those in $Rb_4Cu(MoO_4)_3$ indicating the K-analogue structurally is more distorted than the Rb-analogue, which results in weaker orbital overlap between the d-orbitals of Mo^{6+} and Cu^{2+} and the p-orbital of O^{2-}. Therefore, magnetic correlations between neighboring Cu^{2+} ions in $K_4Cu(MoO_4)_3$ are overall weaker than those in $Rb_4Cu(MoO_4)_3$.

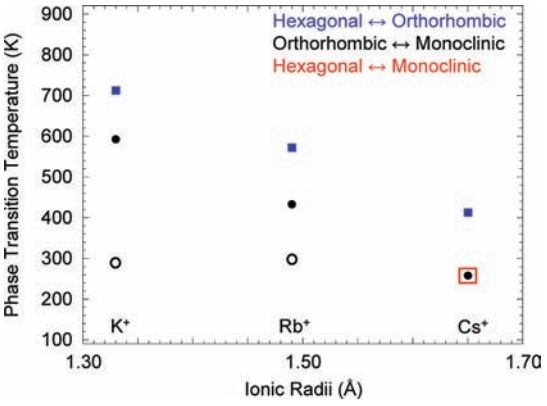

Figure 1. Phase transition temperatures (K) of $A_4Cu(MoO_4)_3$ (A^+ = K^+, Rb^+, Cs^+) as a function of ionic radii (Å) are plotted. Closed markers represent transition temperatures as previously reported,[30] and the open markers represent transition temperatures determined experimentally. Blue squares represent the transition from the hexagonal to the orthorhombic phase, black circles represent the transition from the orthorhombic to the monoclinic phase, and red squares represent the transition from the hexagonal to the monoclinic phase.

Crystal Structure of $K_4Zn(MoO_4)_3$. $K_4Zn(MoO_4)_3$, shown in Figure 4, is modeled in the orthorhombic *Pnma* space group with lattice dimensions of *a* = 10.688(10) Å, *b* = 22.022(6) Å, and *c* = 6.105(10) Å. With the exception of the transition metal environment, the structure of $K_4Zn(MoO_4)_3$ is very similar to that of $A_4Cu(MoO_4)_3$ (*A* = K, Rb). The structure of $K_4Zn(MoO_4)_3$ consists of ZnO_4 tetrahedra surrounded by two slightly distorted MoO_4 tetrahedra along the *c* direction and two distorted MoO_4

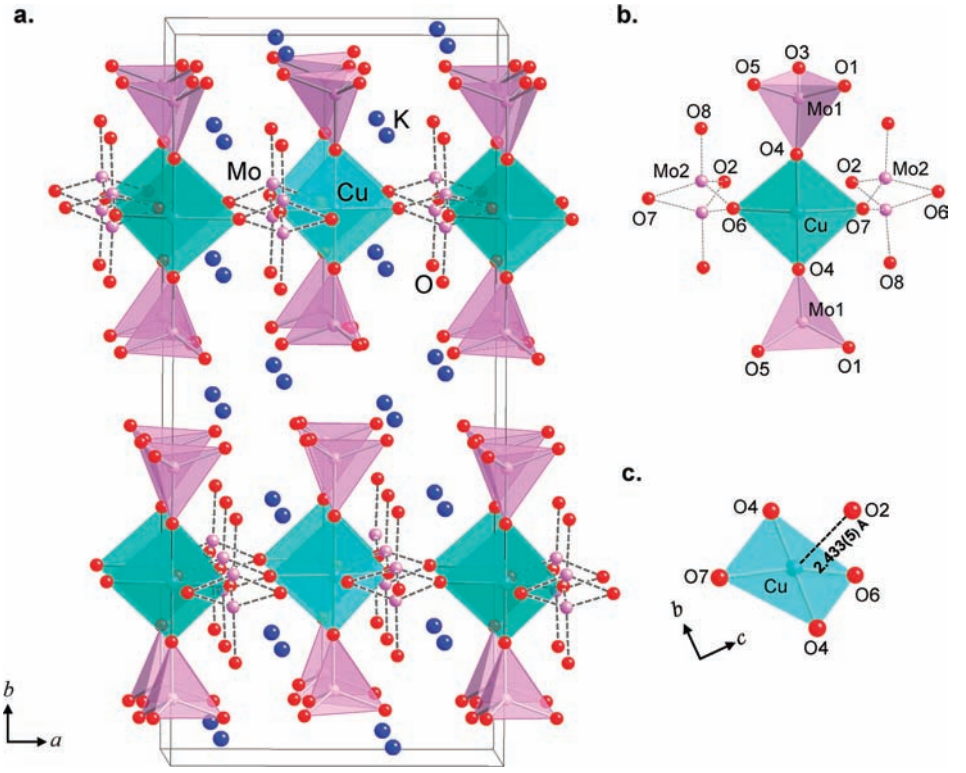

Figure 2. (a) Crystal structure of $K_4Cu(MoO_4)_3$ is shown as blue, green, pink, and red spheres representing K, Cu, Mo, and O atoms, respectively. (b) The distorted Cu^{2+} square planar environment is shown with the surrounding Mo-centered moieties. (c) A view of the puckered Cu^{2+} square planar environment. The dashed lines represent bonds from partially occupied Mo atoms.

dx.doi.org/10.1021/ic200476n |*Inorg. Chem.* 2011, 50, 8767–8773

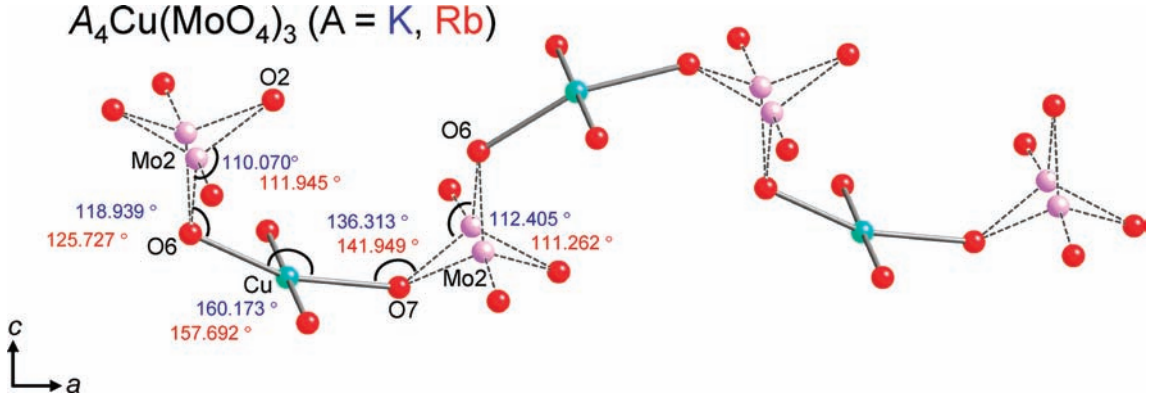

Figure 3. Cu^{2+} quasi-1-d chains of both $K_4Cu(MoO_4)_3$ and $Rb_4Cu(MoO_4)_3$ are shown with the bond angles for $K_4Cu(MoO_4)_3$ in blue and $Rb_4Cu(MoO_4)_3$ in red. The dashed lines represent bonds from partially occupied Mo atoms.

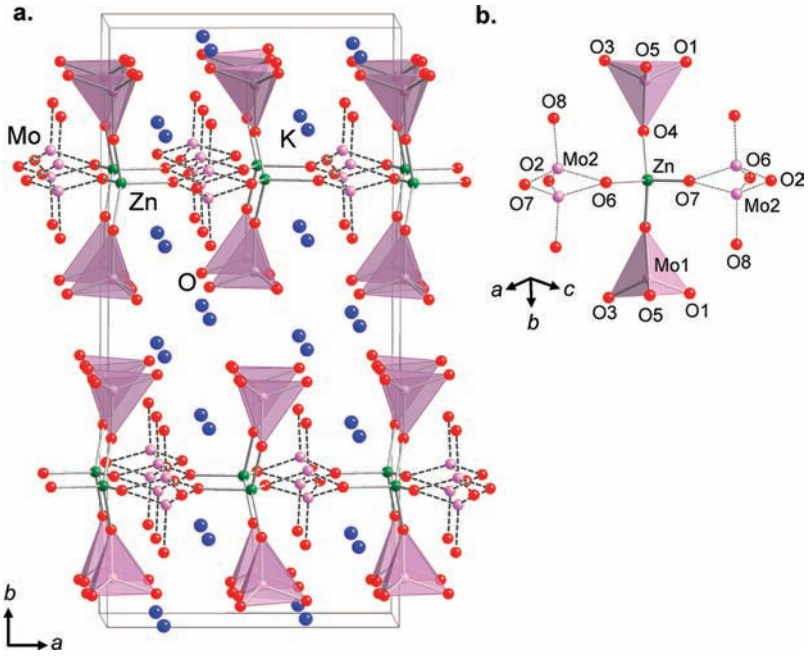

Figure 4. (a) Crystal structure of $K_4Zn(MoO_4)_3$ is shown as blue, green, pink, and red spheres representing K, Zn, Mo, and O atoms, respectively. (b) A view of the Zn^{2+} environment is shown with the surrounding Mo-centered moieties. The dashed lines represent bonds from partially occupied Mo atoms.

tetrahedra, with Mo2 and O8 partially occupied (0.5), along the *ab*-plane. As shown in Figure 4b, the ZnO_4 tetrahedra are coordinated to four distorted MoO_4 tetrahedra with two crystallographically distinct Mo sites. The distortions in the MoO_4 tetrahedra and ZnO_4 tetrahedra can also be understood using electronic considerations similar to that found in $A_4Cu(MoO_4)_3$ (A = K, Rb) and account for the longer Zn−O contacts in the *ac*-plane and the shorter Zn−O contacts along the *b*-axis.

Magnetic Properties of $K_4Cu(MoO_4)_3$. The temperature dependence of the magnetic susceptibility was investigated at B = 0.01 and 7 T for B // *ac* and B // *b* in the range of 2−350 K with the low temperature data (0−50 K) shown in Figure 5. The magnetic susceptibility was measured across the structural transition (∼280 K) with no indication of a magnetic transition, similar to the magnetic susceptibility of $Rb_4Cu(MoO_4)_3$.[15] The temperature-dependent polymorphs of $Rb_4Cu(MoO_4)_3$ are structurally very similar to each other and are built of the same structural moieties.

The magnetic susceptibility data were corrected for core electron diamagnetism in $K_4Cu(MoO_4)_3$, and the diamagnetic contribution to the magnetic susceptibility has been determined to be $\chi_{dia} = -2.88 \times 10^{-4}$ emu/mol.[34] No bifurcation was observed between ZFC and FC magnetic susceptibility measurements down to 0.01 T, which indicates that $K_4Cu(MoO_4)_3$ does not show the spin freezing behavior characteristic of a spin-glass system. The difference between B // *ac* and B // *b* susceptibility is attributable to the anisotropy of the *g*-value and the Van Vleck's paramagnetism. The $\chi(T)$ data were fit with $\chi(T) = \chi_0 + C / (T - \Theta_W)$ (C = Curie−Weiss constant) for 35−350 K at 0.01 T. The experimental effective moment p_{eff}, *g*-value, Weiss temperature Θ_W, and constant term χ_0 are shown in Table 4. χ_0 is most likely due to the Van Vleck paramagnetism by the orbital

dx.doi.org/10.1021/ic200476n |*Inorg. Chem.* 2011, 50, 8767–8773

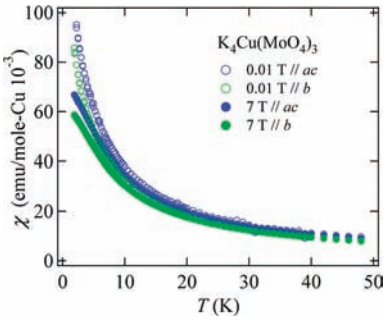

Figure 5. Temperature-dependent magnetic susceptibility of $K_4Cu(MoO_4)_3$ is shown below 50 K. Blue and green, closed and open circles show magnetization B // ac and B // b in 7 and 0.01 T, respectively. No hysteresis is observed between ZFC and FC measurements.

Table 4. Magnetic Properties Of $K_4Cu(MoO_4)_3$

	B // ac	B // b
ρ_{eff} (μ_B)	1.89(1)	1.75(1)
J	3.8	4.6
g	2.18(1)	2.02(1)
Θ_W (K)	−2.32(1)	−1.89(1)
χ_0 (emu/mol)	2.63 x10^{-4}	2.46 x10^{-4}

hybridization. The Weiss temperatures are negative for both directions, which indicate antiferromagnetic interactions between neighboring Cu^{2+} ions. While the p_{eff} for B // b is close to the theoretical value 1.73 μ_B for Cu^{2+} spin-1/2, the p_{eff} for B // ac is larger than expected, which can be attributed to spin−orbital coupling. The p_{eff} and g-values for B // b are consistent with that found for $Rb_4Cu(MoO_4)_3$.[15] However, the p_{eff} and g-values for B // ac are slightly smaller than those for $Rb_4Cu(MoO_4)_3$, which is consistent with weaker coupling between the Cu−O−Mo chains. The magnetic anisotropy in $K_4Cu(MoO_4)_3$ is smaller than that found in $Rb_4Cu(MoO_4)_3$, which is consistent with weaker orbital overlap, as discussed in the structure section above. Θ_W for B // ac and B // b is smaller in $K_4Cu(MoO_4)_3$ than those of $Rb_4Cu(MoO_4)_3$. The exchange interactions in $K_4Cu(MoO_4)_3$ are estimated to be J ~4.6 K and 3.8 K from $\Theta_W = -[zs(s+1)J]/3$ (z = 2 is the number of nearest-neighbor magnetic ions) for a spin-1/2 1-d antiferromagnetic chain. The broad peak in χ associated with the development of short-range order is not observed down to 2 K due to the small exchange interaction in $K_4Cu(MoO_4)_3$. The characteristic broad peak in $\chi(T)$ for a 1-d antiferromagnetic chain is known to appear at $T \sim 0.6J \sim \Theta_W$.[36] The absence of a leveling off feature toward the lowest temperature (2 K) of the susceptibility measurement at 0.01 T suggests a small inclusion (~several %) of Curie component of S = 1/2. For a quantum spin chain system, this type of free spin may often appear due to the imperfections of the structure, such as defects, edge of the chain, etc.

Figure 6 shows the field-dependent magnetization up to 7 T measured at 2 K for B // ac and B // b. No hysteresis is observed between up-sweep and down-sweep measurements. Field-dependent magnetization at 2 K has a convex curvature. At temperatures below 2 K, however, the field-dependent magnetization may have a concave curvature attributable to the characteristic decrease of spin moment due to strong quantum fluctuations expected for a spin-1/2 quantum spin system such as

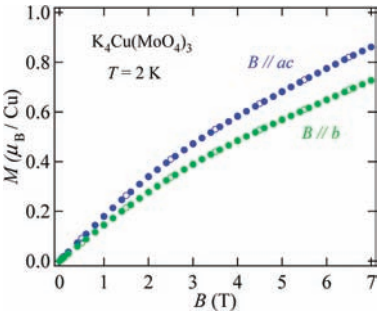

Figure 6. Field-dependent magnetization at 2 K of a single crystal of $K_4Cu(MoO_4)_3$ was measured up to 7 T for B // ac and B // b. Closed and open circles indicate the up-sweep and down-sweep measurements, respectively.

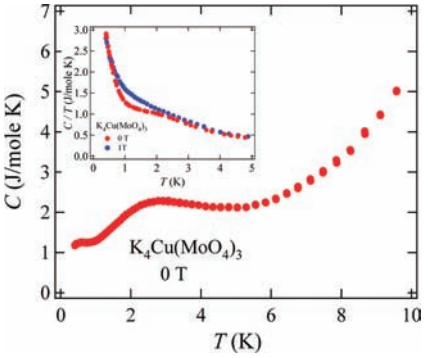

Figure 7. Temperature dependence of the specific heat, C, at 0 T of a single crystal of $K_4Cu(MoO_4)_3$ was measured down to 0.4 K. Inset: Temperature dependence of C/T at 0 and 1 T of $K_4Cu(MoO_4)_3$ down to 0.4 K.

$K_4Cu(MoO_4)_3$. The magnetic moment at 7 T is about 70% of the saturation magnetization ~1 μ_B for spin-1/2 and is consistent with the theoretical estimate of the saturation field of 2 J (~13.5 T) using J ~5 K for a 1-d spin-1/2 chain system at T = 0 K.[35]

Finally, Figure 7 shows the specific heat, C/T, of $K_4Cu(MoO_4)_3$ as a function of temperature at 0 T. No sharp anomaly indicating a magnetic long-range order is observed down to 0.4 K. The weak low-T enhancement of C/T below 1 K is seen in the inset of Figure 7 and is attributable to the Schottky contribution from the free moment of (Cu^{2+}) S = 1/2 with a volume fraction of 9.9%.[36] Notably, there is a broad peak at ~2.3 K (~Θ_W), which may be attributed to the development of short-range ordering. Indeed, the 1-d quantum spin chain systems are expected to form a broad peak in $C(T)$ at $T \sim 0.5J$, and it is indeed the case here, providing evidence that most likely the system forms a quantum spin liquid state below ~2.3 K.[37]

CONCLUSIONS

We report the crystal structure and magnetic properties of a new quasi-1-d quantum antiferromagnet, $K_4Cu(MoO_4)_3$, and the crystal structure of its nonmagnetic reference, $K_4Zn(MoO_4)_3$. In comparison with the increased structural distortion along the Cu−O−Mo chains, the results in weaker orbital overlap between chains due to the increased Cu−O2 distance and along the Cu−O−Mo chains due to decreased Cu−O−Mo bond angles, and the increase in distortion along the chains weakens the magnetic exchange interaction in $K_4Cu(MoO_4)_3$

dx.doi.org/10.1021/ic200476n |Inorg. Chem. 2011, 50, 8767–8773

($J \sim 4-5$ K) as compared to that in $Rb_4Cu(MoO_4)_3$ ($J \sim 10$ K). This decrease in the coupling, J, results in a suppression below 2 K of the broad peak expected for 1-d spin chains in magnetic susceptibility and is confirmed in specific heat measurements.[38] Therefore, both $K_4Cu(MoO_4)_3$ and $Rb_4Cu(MoO_4)_3$ can be described as quantum spin-1/2 1-d antiferromagnets with a likely quantum spin liquid ground state.

■ ASSOCIATED CONTENT

Supporting Information. Crystallographic information files (CIF) and a plot of the volume of $K_4Cu(MoO_4)_3$ as a function of temperature (Figure S1). This material is available free of charge via the Internet at http://pubs.acs.org.

■ AUTHOR INFORMATION

Corresponding Author

*Tel: +1-225-578-2695. Fax: +1-225-578-3458. E-mail: jchan@lsu.edu.

■ ACKNOWLEDGMENT

We acknowledge Keisuke Onuma and Yoshiteru Maeno for their contribution and useful discussions. J.Y.C. and M.C.M. acknowledge NSF DMR-0756281 and 1063735 for financial support of this project and Dr. F. R. Fronczek for useful discussions. This work was partially financially supported by Grant-in-Aid (No. 21684019) from the Japanese Society for the Promotion of Science and also by Grant-in-Aid for Scientific Research on Priority Area (No. 19052003) from the Ministry of Education, Culture, Sports, Science and Technology, Japan.

■ REFERENCES

(1) Haldane, F. D. M. *Phys. Rev. Lett.* **1983**, *50*, 1153–1156.
(2) Yamashita, M.; Ishii, T.; Matsuzaka, H. *Coord. Chem. Rev.* **2000**, *198*, 347–366.
(3) Affleck, I. J. *J. Phys.: Condens. Matter* **1989**, *1*, 3047–3072.
(4) Anderson, P. W. *Science* **1987**, *235*, 1196–1198.
(5) Tsujimoto, Y.; Kitada, A.; Uemura, Y. J.; Goko, T.; Aczel, A. A.; Williams, T. J.; Luke, G. M.; Narumi, Y.; Kindo, K.; Nishi, M.; Ajiro, Y.; Yoshimura, K.; Kageyama, H. *Chem. Mater.* **2010**, *22*, 4625–4631.
(6) Nakatsuji, S.; Nambu, Y.; Tonomura, H.; Sakai, O.; Jonas, S.; Broholm, C.; Tsunetsugu, H.; Qiu, Y.; Maeno, Y. *Science* **2005**, *309*, 1697–1700.
(7) Giamarchi, T.; Ruegg, C.; Tchernyshyov, O. *Nat. Phys.* **2008**, *4*, 198–204.
(8) Knetter, C.; Muller-Hartmann, E.; Uhrig, G. S. *J. Phys.: Condens. Matter* **2000**, *12*, 9069–9083.
(9) Lang, M.; Bruhl, A.; Pashchenko, V.; Removic-Langer, K.; Tsui, Y.; Tutsch, U.; Wolf, B.; Kretz, T.; Lerner, W.; Wagner, M.; Schreuer, J. *J. Phys.: Conf. Ser.* **2006**, *51*, 1–8.
(10) Dagotto, E.; Rice, T. M. *Science* **1996**, *271*, 618–623.
(11) Colman, R. H.; Ritter, C.; Wills, A. S. *Chem. Mater.* **2008**, *20*, 6897–6899.
(12) Alves, L. M. S.; Damasceno, V. I.; dos Santos, C. A. M.; Bortolozo, A. D.; Suzuki, P. A.; Filho, H. J. I.; Machado, A. J. S.; Fisk, Z. *Phys. Rev. B* **2010**, *81*, 174532.
(13) Torardi, C. C.; McCarley, R. E. *J. Solid State Chem.* **1981**, *37*, 393–397.
(14) Ramanujachary, K. V.; Greenblatt, M. *J. Solid State Chem.* **1993**, *102*, 69–78.
(15) Ishii, R.; Gautreaux, D.; Onuma, K.; Machida, Y.; Maeno, Y.; Nakatsuji, S.; Chan, J. Y. *J. Am. Chem. Soc.* **2010**, *132*, 7055–7061.
(16) da Luz, M. S.; dos Santos, C. A. M.; Moreno, J.; White, B. D.; Neumeier, J. J. *Phys. Rev. B* **2007**, *76*, 233105.
(17) Greenblatt, M. *Chem. Rev.* **1988**, *88*, 31–53.
(18) Trunov, K.; Efremov, V. A.; Velikodnyi, Y. A. *Nauka Tekh. (Leningrad)* **1986**, 25–170.
(19) Gicquel-Mayer, C.; Mayer, M.; Perez, G. *Chem. Minerale* **1980**, *17*, 445–457.
(20) Gicquel-Mayer, C.; Mayer, M.; Perez, G. *Chem. Minerale* **1976**, *283*, 533–535.
(21) Solodovnikov, S. F.; Klevtsova, R. F.; Glinskaya, L. A.; Klevtsov, P. V. *Kristallografiya* **1988**, *33*, 1380–1386.
(22) Solodovnikov, S. F.; Klevtsova, R. F.; Klevtsov, P. V. *J. Struct. Chem.* **1994**, *35*, 879–889.
(23) Solodovnikov, S. F.; Klevtsova, R. F.; Glinskaya, L. A.; Klevtsov, P. V. *Zh. Neorg. Khim.* **1994**, *39*, 1942–1947.
(24) Solodovnikov, S. F.; Klevtsova, R. F.; Glinskaya, L. A.; Klevtsov, P. V. *Kristallografiya* **1988**, *33*, 1380–1386.
(25) Sarma, D. D. *Curr. Opin. Solid State Mater. Sci.* **2001**, *5*, 261–268.
(26) Huang, Y.-H.; Liang, G.; Croft, M.; Lehtimäki, M.; Karppinen, M.; Goodenough, J. B. *Chem. Mater.* **2009**, *21*, 2319–2326.
(27) Solodovnikov, S.; Solodovnikova, Z. A. *J. Struct. Chem.* **1997**, *38*, 765–771.
(28) Svistov, L. E.; Smirnov, A. I.; Prozorova, L. A.; Petrenko, O. A.; Demianets, L. N.; Shapiro, A. Y. *Phys. Rev. B* **2003**, *67*, 094434.
(29) Ishii, R.; Tanaka, S.; Onuma, K.; Nambu, Y.; Tokunaga, M.; Sakakibara, T.; Kawashima, N.; Maeno, Y.; Broholm, C.; Gautreaux, D. P.; Chan, J. Y.; Nakatsuji, S. *Europhys. Lett.* **2011**, *94*, 17001.
(30) Klevtsov, P. V.; Kim, V. G.; Kruglik, A. I.; Klevtsova, R. F. *Kristallografiya* **1989**, *34*, 1475–1479.
(31) Altomare, A.; Burla, M. C.; Camalli, M.; Cascarano, G.; Giacovazzo, C.; Guagliardi, A.; Polidori, G. *J. Appl. Crystallogr.* **1994**, *27*, 435.
(32) Sheldrick, G. M. *Acta Crystallogr., Sect. A: Found Crystallogr.* **2008**, *A64*, 112–122.
(33) Spek, A. L. *J. Appl. Crystallogr.* **2003**, *36*, 7–13.
(34) Selwood, P. W. *Magnetochemistry*; Interscience: New York, 1956.
(35) Griffiths, R. B. *Phys. Rev.* **1964**, *133*, A768–775.
(36) Ramirez, A. P.; Cheong, S.-W.; Kaplan, M. L. *Phys. Rev. Lett.* **1994**, *72*, 3108–3111.
(37) Johnston, D. C.; Kremer, R. K.; Troyer, M.; Wang, X.; Klumper, A.; Bud'ko, S. L.; Panchula, A. F.; Canfield, P. C. *Phys. Rev. B.* **2000**, *61*, 9558–9606.
(38) Eggert, S.; Affleck, I.; Takahashi, M. *Phys. Rev. Lett.* **1994**, *73*, 332–335.